Validation of the Yen–Mullins Model of Athabasca Oil-Sands Asphaltenes using Solution-State 1H NMR Relaxation and 2D HSQC Spectroscopy

ARTICLE *in* ENERGY & FUELS · NOVEMBER 2013

Impact Factor: 2.79 · DOI: 10.1021/ef401412w

4 AUTHORS, INCLUDING:

Rudraksha Dutta Majumdar
University of Toronto
2 PUBLICATIONS **34** CITATIONS

energy&fuels

Article

pubs.acs.org/EF

Validation of the Yen–Mullins Model of Athabasca Oil-Sands Asphaltenes using Solution-State ^{1}H NMR Relaxation and 2D HSQC Spectroscopy

R. Dutta Majumdar,[†,‡] M. Gerken,[†,‡] R. Mikula,[§,∥] and P. Hazendonk*[,†,‡]

[†]Department of Chemistry and Biochemistry, University of Lethbridge, Alberta T1K 3M4, Canada

[‡]Canadian Centre for Research in Advanced Fluorine Technologies, University of Lethbridge, Alberta T1K 3M4, Canada

[§]Kalium Research, 12515 39th Ave., Edmonton, Alberta T6J 0N1, Canada

[∥]Natural Resources Canada, CanmetENERGY Laboratory, Devon, Alberta, Canada

Supporting Information

ABSTRACT: The hierarchical Yen–Mullins model of Athabasca oil-sands asphaltene is strongly supported by solution-state ^{1}H NMR relaxation measurements and 2D HSQC-NMR spectroscopy. For the first time, the ^{1}H T_1 and T_2 relaxation behaviors of specific sites in asphaltene molecules have been studied, and it is shown that the relaxation behavior is in agreement with the hierarchical molecule-nanoaggregate-cluster model proposed by Mullins (*Energy Fuels* **2012**, *26*, 3986). The size of the asphaltene nanoaggregate clusters was determined from the biexponential T_2 relaxation behavior of the ^{1}H nuclei. Assignment of overlapping 1D NMR signals was made possible via HSQC methods, where elusive hallmark long-range aromatic–aliphatic heteronuclear correlations were observed. Alicyclic structures were shown to be more closely associated with the aromatic core than what has been proposed for most archipelago-type structures. The NMR parameters obtained from the deconvolution analysis indicate an average of 6–7 pericondensed aromatic rings present in each molecule, in agreement with the island model. The average molecular weight was determined at ∼720 g/mol, which would be typical for island model structures, hence lending strong support for the Yen–Mullins model.

1. INTRODUCTION

Asphaltenes can be found in all forms of petroleum and hence in all heavy oils and bitumen derived from the Athabasca oil-sands. They are regarded as the heaviest fraction of crude oil[1,2] defined or classified on the basis of their solubility. The components of crude-oil or bitumen that are insoluble in *n*-heptane or *n*-pentane, yet dissolve in toluene, belong to this fraction.[1−4] Since any one specific chemical structure is inadequate to completely describe them, asphaltenes are often proposed to be a complex mixture of aromatic molecules surrounded or linked by aliphatic chains and hetero atoms such as oxygen, sulfur, and nitrogen, as well as metals V, Ni, and Fe.[5] These complex molecules have been reported to form micelles or aggregates within the crude oil leading to precipitation of asphaltene clusters during all the different stages of oil production, causing blockage of well-bore, plugging of pipelines, and also deactivation of catalysts used during refining of the crude.[4,6] One way to avoid precipitation is through flocculation inhibitors, which form a steric repulsive layer around an asphaltene core. Since the action of these inhibitors depends largely on the chemical nature and physical structure of the asphaltene molecules,[7−9] knowledge about chemical and physical properties of asphaltenes is of utmost importance to predict and subsequently prevent the problems caused by asphaltene aggregation. Moreover, bitumen owes many of its physical and chemical properties to its asphaltene content. Detailed knowledge of asphaltene structure would facilitate the development of more efficient and cleaner bitumen processing techniques.

A plethora of analytical techniques have been employed to characterize asphaltenes, which were reviewed by Ancheyta et al.[3] Numerous possible average structures have been proposed,[1,4,10−16] which agree on several aspects but also contradict each other on several issues. O. C. Mullins, in his review,[17] lists several of the major concerns that have either been resolved in the past decade or are still subject to debate, such as average molecular weight, the number of polycyclic aromatic hydrocarbons (PAH) per asphaltene molecule, and the number of fused rings per PAH. A few decades of extensive research have pared down the possible structural models for asphaltenes to two candidates. One of these is the "island" or Yen–Mullins model,[13,14,17] which posits that asphaltene molecules are composed of a large PAH core with pendant aliphatic chains. The second, "archipelago", model[15,16,18] proposes that several smaller PAH units are interconnected via aliphatic tethers. Hence, the question remains, which of these two motifs predominates asphaltene structure?

Solution-state NMR spectroscopy has been essential in developing the current structural motifs for asphaltenes and thus features prominently in the asphaltene literature.[1,4,6,12,19−25] The majority of solution-state NMR spectroscopic studies on asphaltenes are based on one-dimensional techniques such as ^{1}H, ^{13}C, and ^{13}C DEPT (Distortionless Enhancement by Polarization Transfer)[26] NMR spectrosco-

Received: July 22, 2013
Revised: October 15, 2013
Published: October 21, 2013

dx.doi.org/10.1021/ef401412w | *Energy Fuels* 2013, 27, 6528–6537

py.[1,3,6,21] Owing to the large variations in carbon and proton environments within the asphaltene system, the signals are frequently misassigned, especially if they relied solely on the one-dimensional methods. Two-dimensional (2D) NMR correlation techniques are well-known to enable more reliable assignments, but a survey of the literature revealed that 2D NMR spectroscopy has been used sparingly in asphaltene characterization. A few studies used ^{1}H diffusion-ordered spectroscopy (DOSY) experiments for analysis of aggregation behavior in asphaltenes and to determine the size of fused aromatic core.[27−29] Sarpal et al.[30] used 2D-COSY and HETCOR to characterize hydrocracked base stocks of petroleum, which are much lower in molecular weight, composed mostly of the paraffinic fractions and which are fundamentally distinct from asphaltenes as they are products of the cracking process. Moreover, recently it was demonstrated that thermal cracking produce archipelago-type structures.[31] Sarpal's findings[30] were subsequently used by Sheremata et al.[18] to assign the ^{1}H and ^{13}C resonances of asphaltene NMR spectra. Similar 2D approaches were taken by Abu-Dagga et al.[32] and Dosseh et al.[33] to identify and characterize aromatic structures of crude oil components with low and intermediate boiling points, respectively.

Proton and ^{13}C NMR solvent relaxation studies are frequently used to probe aggregation behavior of asphaltenes with increasing asphaltene concentration.[34−36] A few studies rely on direct relaxation measurement on the asphaltene molecules themselves. Pekerar et al.[37] presented ^{13}C T_1 measurements in solution to investigate the mobilities of asphaltene molecules; however, T_1 values alone cannot provide a complete description of the mobility unless they are accompanied by T_2 measurements, as both are required to determine the regime of the motional time-scale. Östlund et al.[38] studied asphaltene flocculation with ^{1}H T_1 and T_2 measurements on the asphaltene molecules directly. This study used only a single peak to represent the aliphatic region in the ^{1}H NMR spectrum, which inherently overlooks the role of underlying signals that have markedly different relaxation behavior. Predictably, their analysis revealed two different T_2 relaxation times of 0.6 and 7.0 ms attributed to protons that are either close or far from the aromatic core, providing little insight into the molecular architecture.

In this fresh look into asphaltene structure by NMR spectroscopy, we provide an in-depth ^{1}H T_1 and T_2 relaxation analysis accompanied by a reexamination of the ^{1}H and ^{13}C spectral assignments aided by HSQC methods. Relaxation at specific sites in asphaltene molecules will depend strongly on the size of the aromatic core and the arrangement of these molecules in solution. Both of these aspects are markedly different for the two proposed models, island and archipelago, and therefore are expected to be instrumental in distinguishing between them.

2. EXPERIMENTAL DETAILS

2.1. Asphaltene Extraction. Bitumen samples from the Athabasca oil-sands were obtained from Natural Resources Canada, CanmetENERGY Laboratory at Devon, Alberta. The asphaltenes were extracted from the bitumen by stirring in *n*-heptane for 2 h at 60 °C and continued stirring at room temperature for 12 h. The resulting solution was suction filtered, and the insoluble part containing the asphaltenes was dissolved in toluene at 50 °C and subsequently filtered. The filtrate was dried under an air-stream yielding a black flaky solid, which was ground to a fine powder and dried under dynamic vacuum for several days to remove residual toluene.

2.2. One-Dimensional Experiments. The sample for 1D ^{1}H and ^{13}C NMR spectroscopy was prepared by dissolving 91 mg asphaltene powder in ca. 1 mL deuterated chloroform ($CDCl_3$). Chromium acetylacetonate [$Cr(acac)_3$] (40 mg) was added as a paramagnetic relaxation agent to shorten the carbon longitudinal relaxation times (T_1). All NMR spectra were obtained using a Bruker Avance II 300.13 MHz NMR spectrometer, equipped with a two-channel BBFO 5-mm solutions probe. Experiments were carried out at ambient temperature. The ^{13}C NMR spectrum was collected by using a 30° excitation angle, with inverse-gated proton decoupling during acquisition with a recycle delay of 21 s as 6500 scans. A recycle delay of 1 s was used for the ^{1}H NMR experiment.

2.3. HSQC and Relaxation Experiments. The HSQC (Heteronuclear Single Quantum Coherence) pulse sequence (Figure 1) is an

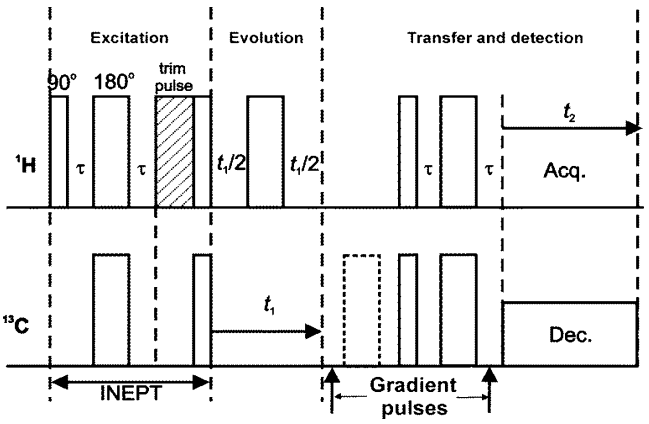

Figure 1. Gradient-selected ^{1}H−^{13}C HSQC pulse sequence used in this paper. The gradient pulses (vertical arrows), with the optional 180° pulse (shown with broken lines) on ^{13}C, only select a coherence pathway and do not discriminate between multiple and single quantum coherences. An optional 1 ms trim-pulse in ^{1}H (shaded), used during the excitation (INEPT transfer) period to suppress long-range coherences, was turned off for one of the long-range HSQC experiments. The value of τ is set as $1/4J$ s, where J is the heteronuclear scalar coupling between ^{1}H and ^{13}C; t_1 represents the acquisition time in the indirect dimension, while t_2 represents that in the direct dimension. The delay times are not to scale.

inverse detected (observed via the ^{1}H nucleus) two-dimensional heteronuclear correlation experiment, where the resulting spectrum has ^{1}H chemical shifts in one dimension and chemical shifts of a magnetically active heteronucleus such as ^{13}C or ^{15}N in the second dimension (^{13}C in this case). Correlation peaks observed on the 2D-plot, therefore, have both ^{1}H and ^{13}C chemical shift values, representing protons and carbons that are connected by a single bond.[39] The sequence is normally optimized for small molecules such that only the single-bond correlations are observed. For larger and more complex molecules, rapid relaxation can make observation of correlations difficult, necessitating modification of the pulse sequence. Besides the usual single-bond correlations, multiple-bond ^{1}H−^{13}C correlations were observed in this work by modifying some of the pulse sequence parameters, as described in more detail in section 3.3. The sample for the initial HSQC experiment to observe short-range correlations (henceforth to be referred to as s-HSQC) was prepared by dissolving 80 mg of the asphaltene in 1 mL toluene-d_8. The experiment was carried out at 60 °C, and no relaxation agent was added. An elevated temperature was used, as room temperature did not provide the desired resolution for some of the correlations. The sample for the HSQC experiment to observe long-range correlations (henceforth to be referred to as l-HSQC) and the ^{1}H T_1 and T_2 measurements was prepared by dissolving 60 mg of asphaltene in approximately 1 mL of $CDCl_3$, without any relaxation agent. A standard Carr−Purcell−Meiboom−Gill (CPMG)[40] sequence was used for the T_2 experiments, and T_1 were determined via standard inversion

dx.doi.org/10.1021/ef401412w | Energy Fuels 2013, 27, 6528−6537

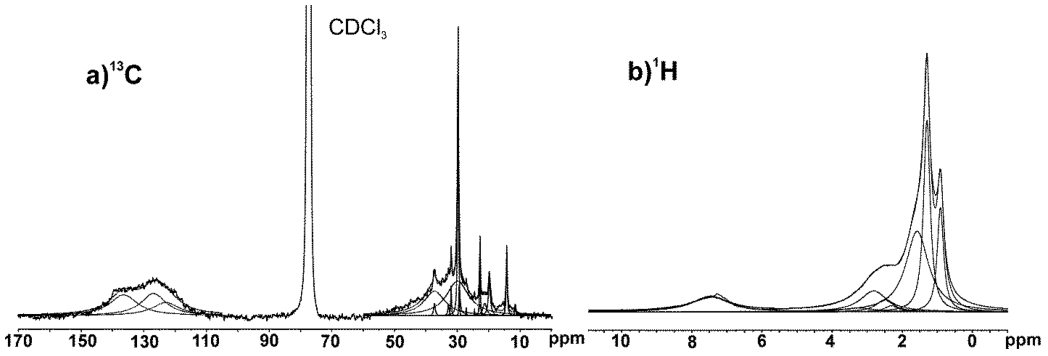

Figure 2. Solution-state (a) $^{13}C\{^{1}H\}$ and (b) ^{1}H NMR spectra of heptane-extracted AOSA in $CDCl_3$, showing the deconvolved peaks. The ^{13}C NMR experiment was carried out with inverse-gated ^{1}H decoupling to obtain a quantitative spectrum. Detailed assignments for all the deconvolved peaks in the ^{13}C and ^{1}H spectra are provided in Tables 1 and 2, respectively.

recovery methods. For the s-HSQC experiment, the sweep widths in both dimensions were optimized to contain just the observable signals (10 ppm for ^{1}H, 150 ppm for ^{13}C). The number transients used in the indirect dimension (TD1) was 128 where 256 scans were recorded for each. A 1-ms trim-pulse was used in the INEPT period to remove long-range couplings. In the l-HSQC experiments, the ^{13}C sweep width (SW) was changed to 400 ppm (30 kHz) and the number of transients in the indirect dimension was reduced to 32 where 1700 scans were recorded for each. The 1 ms trim pulse (see Figure 1 and section 3.3) was retained for one of the l-HSQC experiments while it was turned off for the other by setting its duration to 0 ms. The ^{13}C dimension FIDs in both HSQC spectra were zero filled and forward linear predicted to 1024 points to improve the digital resolution.

All chemical shifts were internally referenced with respect to tetramethylsilane (TMS). The deconvolution analysis was done using the MestRenova software (version 6.0.2). Lorentzian lineshapes were maintained, and the chemical shifts and the line-widths were adjusted to establish a consistent model where the peak heights were allowed to be optimized by the software until minimum residual error was achieved. The presence of overlapping peaks at 22.8 and 37.3 ppm were confirmed by HSQC.

3. RESULTS AND DISCUSSIONS

3.1. Calculation of Structural Parameters Based on Deconvolution Analysis of NMR Spectra. Elemental analysis of Athabasca oil-sands asphaltene (AOSA) provided the relative distribution of the major elements as following: 78.41% C, 8.47% H, 1.12% N, 8% S, and 2% O, which agree closely with reported values.[1,18,22] Figure 2a shows the deconvolved ^{13}C NMR spectrum of AOSA acquired under inverse-gated proton decoupling. Detailed assignment for each signal are shown in Table 1, where a corresponding model is shown in Figure 3 indicating the various carbon sites prescribed by the spectral assignments. The relative contribution from each carbon species was obtained from the peak areas. These distributions were used to compute the number of protons per 100 carbons with the help of eq 1,

$$\text{H per 100 C} = (3 \times \%CH_3) + (2 \times \%CH_2) + \%CH \quad (1)$$

where $\%CH_3$, $\%CH_2$, and %CH are the percentages of methyl, methylene, and methine (including aromatic =C−H) carbons present, respectively. To validate the deconvolution model, the calculated H/C ratio (1.33) was compared to the H/C ratio obtained from elemental analysis (1.30). This 97.7% agreement between their H/C ratios suggests that the peak-fitting model and the assignments of the ^{13}C resonances are accurate. Had the peaks been misassigned, the distribution of the various carbon species would have been markedly different and furthermore have predicted the number of protons to deviate as well. For instance, if the number of CH_3 carbons had been overestimated, it would have led to an increase in the overall number of protons and hence an overestimate of the H/C ratio.

Table 1. Chemical Shift Assignments for the Fitted Peaks of the ^{13}C NMR Spectrum of AOSA

$\delta\{^{13}C\}$ (ppm)	assignment	$\delta\{^{13}C\}$ (ppm)	assignment
11.5, 14.2	terminal (t-) CH_3 on aliphatic chain, at least 3 carbons long	32.0	CH_2 'β' to t-CH_3 or aromatic ring
19.8	branched CH_3, 'β' or more from end of chain	32.8	aliphatic CH
21.3	CH_3 substituent on aromatic ring	37.3[a]	CH_2 or CH 'α' to aromatic ring, CH_2 'α' to branched point in chain
22.8[a]	terminal isobutyl CH_3; CH_2 'α' to t-CH_3	122.9	triple bridgehead quaternary aromatic C
24.5	alicyclic CH_2 'β' to aromatic ring	127.0	aromatic protonated C (CH)
27.2, 29.4, 29.7	aliphatic chain CH_2's more than 'α' or 'β' to aromatic ring	136.4	double bridgehead and substituted quaternary aromatic C
29.9	alicyclic CH_2		

[a]The signals at 22.8 and 37.3 ppm contain contributions from more than one carbon environment as shown by the overlapping fitted peaks in Figure 2a and evidenced by the HSQC spectrum of Figure 5a. The different species of carbons described are illustrated in Figure 3.

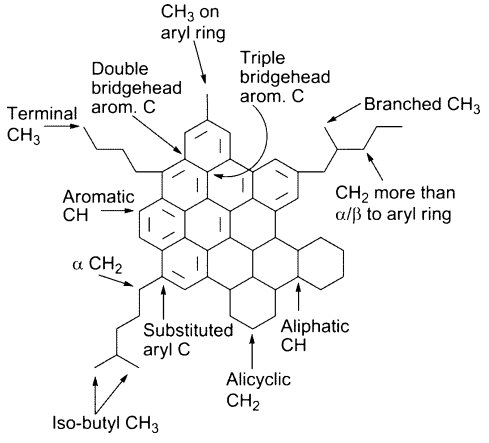

Figure 3. Hypothetical asphaltene molecule showing the different carbon species identified by ^{1}H and ^{13}C NMR spectroscopy, as assigned in Tables 1 and 2.

dx.doi.org/10.1021/ef401412w | Energy Fuels 2013, 27, 6528−6537

The corresponding deconvolution analysis and subsequent calculations were carried out on the ^{1}H NMR spectrum (Figure 2b and Table 2). In this case, the percentage of each species of proton was multiplied by the experimental H/C ratio of 1.3, to enable comparison with the corresponding values obtained from the ^{13}C NMR deconvolution analysis. The number of carbons corresponding to each type of proton was also calculated. Since the number of quaternary aromatic carbons cannot be calculated directly from ^{1}H NMR spectrum, it was obtained by subtracting from 100 the total number of carbons calculated, assuming that there are 100 carbons for every 130 protons (H/C = 1.3).

Table 2. Chemical Shift Assignments for the Fitted Peaks of the ^{1}H NMR Spectrum of AOSA

$\delta\{^1H\}$ (ppm)	assignment	$\delta\{^1H\}$ (ppm)	assignment
0.9	CH_3 not attached to aromatic rings	2.8	aliphatic chain/cyclic CH_2 'α' or 'β' to aromatics
1.3	aliphatic chain CH_2	3.3	CH_2, CH 'α' to aromatic rings under steric strain*
1.6	alicyclic CH_2	7.5	aromatic CH
2.3, 2.5	CH_3 attached to aromatic rings		

*See ref 12.

The number of protons and carbons obtained from both the ^{13}C and ^{1}H spectra are compared in Table 3. The values obtained independently from the two spectra show remarkably good agreement in most cases, proving the self-consistency in the deconvolution models. On average, there are 5−6 CH_3 groups per 100 carbons ($C_{3H,al}$) that are not directly attached to aromatic carbons. Of these, about 2 are branched CH_3 (Figure 3, $\delta\{^{13}C\}$ = 19.8 ppm) and the remaining 3−4 are terminal CH_3, implying 3−4 nonbridging aliphatic chains (more than 1 carbon long) per 100 carbons. The number of methyl groups attached to aromatic carbon ($C_{3H,ar}$) is approximately 2 per 100 carbons. Hence, the number of aromatic carbons substituted by nonbridging aliphatic chains is 5 or 6 per 100 carbons. The number of quaternary aromatic carbons ($C_{quat,ar}$) calculated from ^{13}C NMR spectroscopy is approximately 28, of which 10−11 are triple bridgehead aromatic carbons (junction of three aromatic rings, C_{tb}, $\delta\{^{13}C\}$ = 122.9 ppm). This implies 17−18 quaternary aromatic carbons comprising both substituted (C_{sub}) and double bridgehead aromatic (C_{db}) carbons (since $C_{quat,ar} = C_{tb} + C_{db} + C_{sub}$), both of which appear in the $\delta\{^{13}C\}$ = 136.4 ppm range. Substituted aromatic carbons, (excluding those with attached CH_3) were estimated to be 15 per 100 C by calculating the number of aliphatic carbons 'α' to aromatic rings ($\delta\{^{13}C\}$ = 37.3 ppm). This leads to approximately three C_{db} carbons, which is disproportionately low compared to C_{tb} (≈ 10), since a C_{db}/C_{tb} ratio which is even close to 3/10 is only possible in a highly pericondensed PAH with more than 36 aromatic rings. This apparent discrepancy is removed by reassigning three of the $C_{H,ar}$ groups from the ^{13}C NMR data as C_{db}, making $C_{H,ar}$ and $C_{quat,ar}$ obtained from both ^{13}C and ^{1}H NMR spectroscopy eventually equal (Table 3). This reassignment was done since many of the C_{db} often appear in the $\delta\{^{13}C\}$ = 128−129 ppm region (e.g., coronene, benzo(e)pyrene), lying in the range of $C_{H,ar}$. Later, it will be discussed that asphaltenes are dominated by pericondensed aromatic cores such as coronene and benzo(e)pyrene, which supports this reassignment. Moreover, it turns out that the number of protonated aromatic carbons ($C_{H,ar}$) obtained from ^{13}C and ^{1}H NMR spectra differed by three before reassignment. The double bridgehead aromatic carbons are now approximately 6 per 100 carbons and $C_{H,ar}$ is 14. The H/C ratio was recalculated as 1.29, which is in better agreement with the elemental analysis at 1.30 than the previously calculated ratio of 1.33. Furthermore, the signal at $\delta\{^{13}C\}$ = 37.3 ppm used to determine C_{sub} is significantly broadened to a line width of 608 Hz, implying that aliphatic carbons other than those 'α' to aromatic rings contribute to it. Hence, the value of C_{sub} becomes less than 15, and that of C_{db} ends up being more than 6.

The aromaticity (% aromatic carbon) of the system is 45%, calculated from ^{13}C NMR spectroscopy. It can be broken down as $C_{H,ar} + C_{quat,ar}$. Since $C_{H,ar}$ is 14, $C_{quat,ar}$ comes out to be 31. With C_{tb} being 10 (Table 4), C_{db} and C_{sub} are adjusted so that $C_{db} + C_{sub}$ is always 21 ($C_{quat,ar} = C_{tb} + C_{db} + C_{sub}$), with $C_{db} \geq 6$ and $C_{sub} \leq 15$. The number of aromatic carbons which are substituted by nonbridging aliphatic chains or CH_3 groups is 5 or 6 as discussed previously, setting the lower limit for C_{sub} to 5−6, which is representative of the "island" architecture[41] with no bridging chains. Since the number of aliphatic chain CH_2 groups ($C_{2H,al}$) is about 24−25 per 100 carbon (Table 3), and in case of the island model the number of nonlinking aliphatic chains being 3−4 (not including $C_{3H,ar}$), the average chain length (L) was calculated to be 6−8. This length is in close agreement with chain lengths reported by Cyr et al.[1] and Christopher et al.[21] and lies midway of those reported by Andrews et al.,[25] which show 3-carbon chains on average and a small fraction of 9-carbon chains. It should be noted that this model does not take into account alicyclic substitutions or bridging aliphatic chains, the inclusion of which would result in the prediction of a higher C_{sub} and lower L. If only the bridging

Table 3. Distribution of Different Carbon Species per 100 Carbons and Their Corresponding Protons Calculated Using the Areas under the Fitted Peaks in the ^{13}C and ^{1}H NMR Spectra[a]

	from ^{13}C NMR		from ^{1}H NMR	
functionality	no. C	no. H	no. C	no. H
all CH_3 not attached to aryl carbon	4.9 ± 0.07	14.7 ± 0.21	5.3 ± 0.003	15.9 ± 0.01
CH_3 attached to aryl carbon	1.4 ± 0.13	4.2 ± 0.39	2.5 ± 0.007	7.4 ± 0.02
aliphatic chain CH_2	25.2 ± 0.02	50.4 ± 0.06	23.9 ± 0.005	47.7 ± 0.01
alicyclic CH_2	23.2 ± 0.02	46.4 ± 0.06	22.5 ± 0.002	45.0 ± 0.004
aromatic CH	16.7[b]/13.7[c] ± 0.01	16.7[b]/13.7[c] ± 0.01	14.0 ± 0.01	14.0 ± 0.01
quaternary aromatic C	28.3[b]/31.3[c] ± 0.01		31.8[d]	

[a]Relative errors were calculated with a 3σ corresponding to 99.7% confidence level, obtained from the residual error (χ^2) in the deconvolution analysis. [b]Before reassignment of 3 aromatic CH to quaternary carbons. [c]After reassignment. [d]Calculated by difference.

dx.doi.org/10.1021/ef401412w | Energy Fuels 2013, 27, 6528−6537

Table 4. Average Structural Parameters for AOSA with Distributions per 100 Carbons and per PAH Obtained Using NMR Spectroscopy and Elemental Analysis

structural param.	value for AOSA
C aromaticity (%)	45
C aliphaticity (%)	55
aromatic rings per PAH	6−7
clusters per 100 C	2
aromatic CH per 100 C ($C_{H,ar}$)	14
aromatic CH per PAH	7
triple bridgehead carbons per 100 C (C_{tb})	10−11
triple bridgehead carbons per PAH	5−5.5
substituted aromatic + double bridgehead aromatic carbon per 100 C (C_{sub} + C_{db})	21
substituted aromatic + double bridgehead aromatic carbon per PAH	10.5
total aromatic carbons per PAH	22.5
free aliphatic chains more than one carbon long per 100 C	3−4
free aliphatic chains more than one carbon long per PAH	1.5−2
methyl groups substituted on aromatic ring per 100 C ($C_{3H,ar}$)	2
methyl groups substituted on aromatic ring per PAH	1
C per aliphatic chain (L)	3−8
alicyclic carbons per 100 C	23
alicyclic carbons per PAH	11.5
N atoms per 100 C	1.22
N atoms per PAH	0.61
S atoms per 100 C	3.8
S atoms per PAH	1.9
O atoms per 100 C	1.9
O atoms per PAH	0.9
avg. molar mass of PAH	719.37 g/mol
avg. molar mass per 100 C	1438.74 g/mol

aliphatic chains are considered, each chain corresponding to 2 C_{sub}'s and $6 \leq C_{sub} \leq 15$, there cannot be more than 4 aliphatic linkages per 100 carbons, making $C_{sub} \approx 13-14$ when alicyclic rings substituted on aromatic rings are neglected. This structure would give $L \approx 3$. As discussed subsequently, relaxation measurements and the l-HSQC experiment indicate close association of the alicyclic rings with the aromatic core, thereby reducing the number of possible linking chains. As a large fraction of the carbons are alicyclic (Table 3), the number of aliphatic linkages is most likely to be less than 4 per 100 carbons.

3.2. T_2 and T_1 Relaxation Measurements. The transverse relaxation times (T_2) for the peaks in the ^{1}H NMR spectrum are listed in Table 5. Simply speaking, short T_2's reflect a rigid molecular structure, while long T_2's indicate higher mobility. Each of the signals at $\delta\{^1H\}$ = 0.9, 1.3, 1.6, and 7.5 ppm exhibit biexponential transverse relaxation behavior, with one long and one short T_2 component, indicating that these protons exist in sites with disparate mobilities. The aliphatic chain CH_3 signals at 0.9 ppm are expected to be mobile, with a T_2 of 84.7 ms. The shorter T_2 of 33.3 ms would thus arise from CH_3 groups with some restriction in their motion, which would be steric in origin when explained in terms of the Yen−Mullins model.[17,41] This model proposes that island-type asphaltene molecules form nanoaggregates (<10 aggregation number) via disordered aromatic stacking at concentrations higher than the critical nanoaggregate concentration (CNAC) which is 0.05−0.10 g/L in toluene. At concentrations higher than 2−5 g/L (critical cluster concentration, CCC),[41] these nanoaggregates form

Table 5. Transverse (T_2) and Longitudinal (T_1) Relaxation Times for the ^{1}H NMR Peaks[a]

$\delta\{^1H\}$ (ppm)	assignment	T_2 (ms)	T_1 (s)
0.9	CH_3 not attached to aromatic rings	33.3 (11.6%), 84.7 (88.4%)	0.73, 2.50
1.3	aliphatic chain CH_2	31.8 (9.7%), 59.5 (90.3%)	0.59, 1.50
1.6	alicyclic CH_2	24.9 (21.5%), 86.9 (78.5%)	0.35, 5.00
2.5	CH_3 attached to aromatic rings	64.9	0.55, 7.10
2.8	aliphatic chain/cyclic CH_2 'α' or 'β' to aromatics	24.4	0.42, 7.70
7.5	aromatic CH	30.9 (15.6%), 75.2 (84.4%)	0.69, 2.90

[a]The values in parentheses represent the percentage of protons having the corresponding T_2.

clusters, bringing many of the peripheral aliphatic chains in close proximity (see Figure 1 in ref 41). The sample used in the T_2 measurements had a concentration of 60 g/L, much higher than the CCC, hence clusters are formed. The aliphatic CH_3 groups that are located on the inside, or bulk, of the cluster will therefore exhibit restricted motion and hence have a shortened T_2. The CH_3 groups on the periphery of the cluster will be much less restricted in their mobility, hence possessing longer T_2's. A similar argument applies for the chain CH_2 groups at $\delta\{^1H\}$ = 1.3 ppm, with T_2 values of 59.5 and 31.8 ms. The peripheral CH_2 groups with 59.5 ms T_2 are less mobile than the peripheral CH_3 groups, indicating short aliphatic chain lengths, since CH_2 groups longer chains would have higher mobility.

The long and short T_2 of the alicyclic proton at $\delta\{^1H\}$ = 1.6 ppm are explained in terms of the aforementioned disordered aromatic stacking. If the alicyclic rings are condensed with the aromatic core, they can have two possible conformations with respect to the stacked nanoaggregate, one where they lie inside the stacked core and one where they are on the periphery, as illustrated in Figure 4. Those on the inside will have

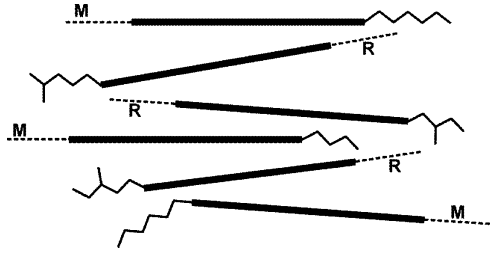

Figure 4. Schematic showing the side view of an asphaltene nanoaggregate formed in solution by disordered aromatic stacking. The thick lines represent the aromatic core while the thinner dashed lines represent the condensed alicyclic rings. The alicyclics labeled 'R' (Rigid) lie within the stacked core and highly rigid with a 24.9 ms T_2. The ones labeled 'M' (Mobile) lie on the periphery of the nanoaggregate and have much higher mobility with a T_2 of 86.9 ms.

significantly reduced mobility compared to those on the periphery, and hence will have much shorter T_2's of 24.9 ms, in comparison to the more mobile ones at 86.9 ms. The CH_3 groups attached to aromatic rings have T_2's at 59.8 ms comparable to the peripheral CH_2 groups at 59.5 ms, indicating that both the moieties lie in the same motional regime. The $\delta\{^1H\}$ = 2.8 ppm signal assigned to CH_2 groups α to aromatic

dx.doi.org/10.1021/ef401412w | Energy Fuels 2013, 27, 6528−6537

rings has 23.4 ms T_2, which is very close to that of the rigid alicyclic protons, suggesting that most of these methylene groups are alicyclic in nature, lying inside the stacked core, as described previously.

Short T_2's (30.9 ms) for the presumably rigid aromatic protons are expected, but to explain the longer T_2 at 75.2 ms, a better appreciation of the relationships among T_2, T_1, and correlation time (τ_c) is required. Correlation times, τ_c, are a measure of the time scale of motion of molecules and are loosely defined as the time required for a molecule to change its orientation over a given angle. When the frequency of reorientational motion (given by $1/\tau_c$) exceeds the Larmor frequency (ω_0), it is said to be in the fast motion regime where the correlation time, $\tau_c < 1/\omega_0$, is considered to be short. Conversely, when the frequency of reorientational motion is significantly slower than ω_0, it is considered to be in the slow motion regime where $\tau_c > 1/\omega_0$. The trends in T_1 and T_2 are similar in the fast motion regime where they gradually decrease with increasing τ_c;[42] however, they diverge upon entering the slow motion regime, where T_1 gradually increases while T_2 decreases asymptotically. Hence, when the T_1 is orders of magnitude larger than T_2, the slow-motion regime applies, which was found to be the case for asphaltenes (Table 5). The longer T_2 and shorter T_1 values in Table 5 represent sites that are less rigid than their shorter and longer counterparts, respectively. The aromatic protons with 75.2 ms T_2 and 0.69 s T_1 therefore belong to the nanoaggregates that are on the periphery of the clusters, making them relatively less rigid than the aromatic protons belonging to nanoaggregates at the center of the clusters, with 30.9 ms T_2 and 2.90 s T_1. Moreover, the T_1/T_2 ratio provides an estimate of time scale of motion. Considering a purely dipolar relaxation model and neglecting chemical shift anisotropy contributions, at very short τ_c (0.001−1.0 ns), that is, when the reorientational motion is very fast (small molecules in low-viscosity liquids), T_1/T_2 approaches unity, and in the case of ^{1}H, the Larmor time scale is 3.3 ns, where T_1/T_2 approaches 2. The T_1/T_2 ratios calculated for asphaltenes range between 4 and 200, which correspond to correlation times between 6 and 52 ns, which are two to 3 orders of magnitude slower than small molecules. This shows that rather than being simple isolated units, asphaltene molecules behave as clusters, which imposes a high degree of restriction on their reorientational motion, which is supportive of the island model.

Estimates of the relative percentages of the rigid and mobile components of each signal was made by using the biexponential behavior of T_2 decay curves and are listed within parentheses in Table 5. These percentages are indicative of the geometry and size of the nanoaggregates and their clusters. The low percentage of rigid aliphatic methyl and methylene groups (11.6 and 9.7%, respectively) indicates that the majority of the aliphatic chains remain on the periphery of the clusters. This in turn implies that the clusters are made up of a small number of nanoaggregates, which is consistent with 15.6% (∼1 in 6) of the nanoaggregates making up the interior of the clusters. Therefore, the number of nanoaggregates per cluster can be predicted as 6 to 7, where the peripheral nanoaggregates have a higher mobility than the internal ones. Furthermore, a relatively higher percentage of rigid alicyclic groups (21.5%) compared to rigid chain aliphatics (9−12%) is indicative of the cyclic groups being more closely associated with the aromatic core.

3.3. HSQC NMR Spectroscopy. A typical two-dimensional experiment constitutes three stages, excitation, evolution or mixing, and detection, and is collected as a series of one-dimensional experiments at different evolution periods. HSQC is an inverse detected 2D pulse sequence (Figure 1); that is, the final detection is done using the ^{1}H nucleus. In the excitation period of HSQC, the ^{1}H nucleus is excited and the resulting magnetization is transferred to ^{13}C, followed by a period of evolution (t_1 in Figure 1), which furnishes the ^{13}C dimension of the spectrum. This period is followed by transferring the magnetization back to ^{1}H for detection, furnishing the ^{1}H dimension. The excitation period is normally optimized to observe single-bond correlations in small molecules, but for a complex system such as asphaltenes, rapid relaxation limits the time window over which correlations can be built-up, impeding the intensity of the correlations observed. For the current study, the sequence was optimized by changing the excitation and evolution periods, to observe single-bond correlations, as well as correlations over multiple bonds, as described below.

The ^{1}H−^{13}C s-HSQC spectrum is shown in Figure 5a, with an expansion of the aliphatic region in the inset. Well-resolved aliphatic (CH_3, CH_2, CH) ^{1}H-to-^{13}C single-bond correlations were observed. The correlations arising from the toluene-d_8 are marked as solvent. Unfortunately these solvent signals overlap with some of the asphaltene correlations in both the aliphatic and aromatic region, which were well-resolved in $CDCl_3$ where the correlations are clearly visible in the l-HSQC (Figure 5b). No correlations between aromatics and aliphatics are seen; hence, any useful information derived from these connectivities between the aromatic core and the aliphatics is lost. Nonetheless, these correlations proved to be invaluable in carrying out the deconvolution analysis, validating the model, as it distinguished overlapping signals such as those at $\delta\{^{13}C\}$ = 22.8 and 37.3 ppm. The signal at $\delta\{^{13}C\}$ = 22.8 ppm contains contributions from two carbon types: terminal isobutyl CH_3 and CH_2 that are α to terminal CH_3. The signals at $\delta\{^{13}C\}$ = 37.3 ppm consists of rigid CH_2 groups α to aromatic rings and the comparatively mobile CH_2 groups α to branched points in a chain. The correlations also helped to validate these assignments since the ^{1}H and ^{13}C chemical shifts of any particular moiety could be verified. Assignments in literature were based solely on the 1D ^{13}C NMR spectrum[12,18] and were verified via their ^{1}H chemical shifts. The broadness of the strongest correlation at $\delta\{^{13}C\}$ = 29 ppm indicates that this aliphatic CH_2 signal consists of a rigid (broad) and mobile (narrow) component, which was subsequently used in the deconvolution analysis.

The absence of aromatic−aliphatic correlations in Figure 5a, however, does not imply that such connectivities are absent in the asphaltene molecules. Any aromatic−aliphatic heteronuclear correlation results from multiple-bond, ^2J or ^3J C−H couplings. The intensity of the magnetization transferred from ^{1}H to ^{13}C in the INEPT transfer segment of the HSQC sequence is modulated as $\sin(2\pi J\tau)$,[43] where J is the heteronuclear scalar coupling constant in Hz and 2τ is the total transfer period (Figure 1). Hence, the ^{1}H−^{13}C single-bond correlations with stronger J coupling (typically 145 Hz) build up magnetization much faster than the weakly coupled (0−60 Hz) multiple (2−3) bond correlations, as illustrated in Figure 6a. For the typical J value, $\tau = 1/4J$ gives the maximum transfer efficiency. In a routine HSQC experiment, as in the s-HSQC, τ = 1.72 ms is used, corresponding to J = 145 Hz, because only single-bond correlations are desired. At this short value of τ, the multiple-bond correlations are much weaker, as evident from Figure 6a. Moreover, a 1-ms trim-pulse on ^{1}H

dx.doi.org/10.1021/ef401412w | Energy Fuels 2013, 27, 6528−6537

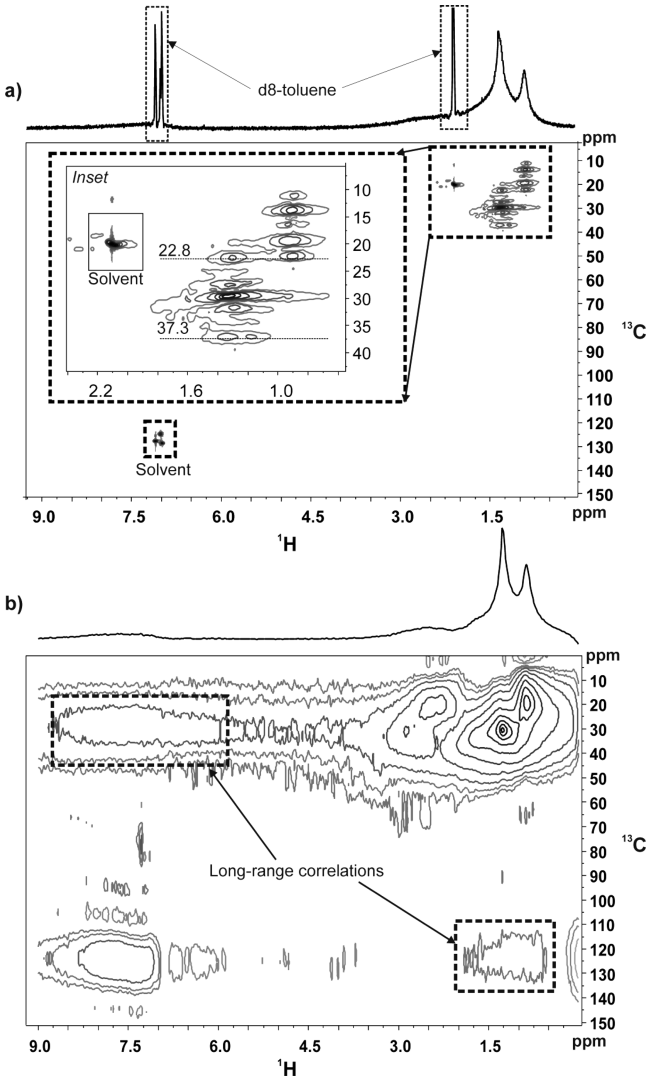

Figure 5. ^{1}H−^{13}C HSQC NMR spectra of heptane extracted AOSA. Acquired with (a) ^{13}C SW = 150 ppm, TD1 = 128, and 256 scans and (b) ^{13}C SW = 400 ppm, TD1 = 32, and 1700 scans. The 1-ms trim pulse was on for both. Experiment a was done at 60 °C in d8-toluene while b was done at room temperature (rt) in $CDCl_3$. (a) Inset: Magnification of the aliphatic region, showing the signals (22.8 and 37.3 ppm ^{13}C dimension) that contain overlapping peaks in the 1D ^{13}C NMR spectrum. Aliphatic−aromatic long-range correlations are highlighted (dashed boxes) in b.

(Figure 1) during the INEPT transfer is implemented to remove long-range effects. The INEPT period is followed by a period of evolution t_1 where the coherences are labeled by their corresponding ^{13}C chemical shift, providing the ^{13}C dimension in the spectrum. The intensity of magnetization in this period is modulated as $\cos(\Omega_C t_1)$, where Ω_C is the carbon chemical shift offset in Hz and transverse (T_2) relaxation is also in effect, which leads to gradual decay as illustrated in Figure 6b. Gradient pulses are used at this stage (Figure 1) to generate a spectrum with absorption mode line shapes by proper coherence pathway selection.[44] It is clear from Figure 6b that if t_1 is sufficiently long, the long-range correlations are hardly detectable, while the short-range ones still have appreciable intensity. Also, the shorter the T_2 of a signal is, the faster it will decay. Hence, to observe the long-range correlations, the t_1 needs to be shortened such that the long-range correlations can

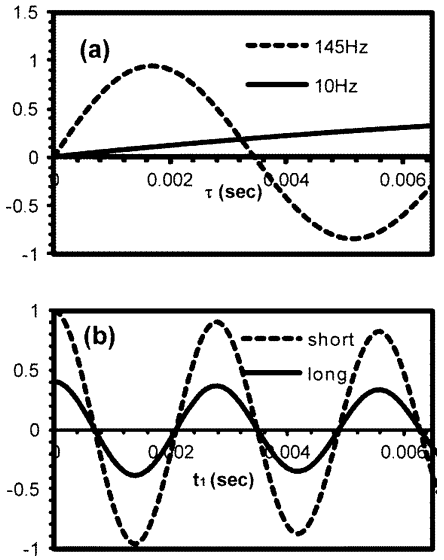

Figure 6. (a) Modulation of the intensity of magnetization transfer by ^{1}H−^{13}C *J*-coupling as a function of the INEPT transfer period (τ) of Figure 1; (b) modulation of the short and long-range correlations after magnetization transfer as a function of the acquisition period in the indirect (^{13}C) dimension. The short and long-range correlations correspond to 145 and 10 Hz *J*-coupling, respectively, of a.

be observed at or close to their maximum intensity. This can be done by reducing TD1 (number of increments in the indirect dimension) and increasing SW (^{13}C sweep width) since t_1 = TD1/(2SW) (see section 2.3). However, the effect of the aforementioned 1-ms trim-pulse should not be overlooked. If it is efficient then it should ideally remove all long-range coupling effects and no aromatic−aliphatic correlations should be observable. To test this, two separate l-HSQC experiments were carried out, one with (Figure 5b) and one without (see Supporting Information) the trim pulse. The t_1 of 6 ms used for the s-HSQC experiment was reduced to 0.5 ms for l-HSQC, which reduces the digital resolution due to a smaller TD1, but a much higher number of scans were recorded (see Experimental Details) to increase the signal-to-noise ratio. Now, the total evolution period (4τ + trim-pulse + t_1, not considering the gradient pulses) for the l-HSQC sequences with and without the trim pulse are 8.38 and 7.38 ms, respectively, which are much lower than the T_2 values reported earlier (shortest T_2 = 24.4 ms). The same for the s-HSQC sequence with the trim-pulse as 13.9 ms. Using these modified parameters, it was observed that both the l-HSQC sequences, with and without the trim-pulse, give very similar spectra, both showing long-range aromatic−aliphatic correlations. The trim-pulse omitted l-HSQC spectrum (see Supporting Information) shows slightly more intense long-range correlations than the one where the trim pulse was retained (Figure 5b), showing that the trim-pulse does filter out some of the long-range heteronuclear couplings but not efficiently enough. These correlations are not observed in the s-HSQC experiment due to its longer evolution period, where the long-range signals are dephased. The evolution period t_1 is longer because of higher number of increments and a shorter sweep-width. Thus, rather than the trim-pulse, it is largely the acquisition time in the indirect dimension that determines which signals survive the sequence to be detected.

The above discussion shows that the effective long-range (^{2}J, ^{3}J) C−H couplings between the aromatic core and aliphatic

dx.doi.org/10.1021/ef401412w | *Energy Fuels* 2013, 27, 6528−6537

substituents are significantly stronger than what is found in regular, well-defined molecules.[45] It is already established that all segments of asphaltene molecules lie in the slow motion regime, among which some segments are structurally more rigid than others. The structural rigidity inhibiting the motional averaging of heteronuclear dipolar couplings and ^{1}H spin-diffusion between proximal segments of the molecules make the effective coupling stronger than standard long-range scalar couplings, the effect being more pronounced for the more rigid segments. It results in better magnetization transfer during the INEPT period of the HSQC sequence. It is reasonable to postulate that alicyclic rings condensed with the aromatic core would be structurally more rigid than chain aliphatics. Also, as shown earlier using T_2 relaxation, a majority of the rigid aliphatics proximal to the aromatic core are the alicyclic rings. Thus, the long-range aromatic−aliphatic correlations observed in the l-HSQC spectrum are mostly due to the rigid alicyclic segments of the asphaltene molecules, which are condensed with the aromatic core.

3.4. Determination of Aromatic Core Size and Final Structure. The model proposed here closely resembles the island model, with aromatic rings with condensed with alicyclic rings. The aromatic cores are substituted by pendant aliphatic chains that are 3−6 carbons long. A small number of linked archipelago type structures may be present and cannot be ruled out completely, as they have been shown to be present in previous studies.[16,29] The number of linking aliphatic chains, however, are not expected to be as high as the structures proposed by Sheremata et al.[18] which was later refined by Boek et al.[46] in support of the island model. The size of the aromatic core can be determined by using a protocol developed by Solum et al.,[47] which was later used by Andrews et al.[25] They plot the mole fraction of bridgehead aromatic carbons χ_b (ratio of bridgehead carbons to the aromaticity) versus the number of carbons per PAH, using equation 18 in ref 47; χ_b can be easily calculated using the NMR data and its value can be used to obtain the number of carbons per PAH from the plot. As established earlier, in our case, $C_{tb} \approx 10$ and $6 \leq C_{db} \leq 15$, putting the total bridgehead carbon value between 16 and 25. The aromaticity being 45, we get $0.36 \leq \chi_b \leq 0.56$, which corresponds to 16−30 aromatic carbons per PAH, that is, between 4 and 9 aromatic rings per PAH with pericondensed structures dominating and no purely catacondensed structures present (refer to Figure 6 in ref 47). Hence, the average PAH size is 6.5, that is, 6−7 aromatic rings, and the number of PAHs per 100 carbons is 1.9. For the sake of calculation, the average number of PAHs per 100 carbons can be rounded to two and all the corresponding structural parameters have been listed in Table 4. Each PAH of 6−7 pericondensed rings has two to three aliphatic chain substitutions, including CH_3 groups substituted on aryl rings. The average length of the aliphatic chains can vary between 3 and 8, subject to the presence of bridging chains. If bridging structures are present, the average chain length will be on the shorter side. Based on elemental analysis results, there appear to be approximately 1 N, 2 S, and 1 O atom per PAH. This PAH size of ∼7 rings is consistent with several other older and more recent studies using a variety of techniques such as scanning tunneling microscopy,[48] high-resolution transmission electron microscopy,[49] electronic triplet-state spectroscopy,[50] and time-resolved fluorescence depolarization.[24,51−53] All of these studies support the island molecular architecture. Moreover, as discussed previously, the relaxation behavior of the asphaltenes can be explained in light of the Yen−Mullins model. The average molecular mass of a PAH based on all these parameters was calculated to be approximately 720 g/mol. It lies in the molecular weight range of 500−1000 g/mol as reported by most mass spectroscopic[14,51,54] and diffusion studies.[13,52,55−57] Mass spectrometry is known to suffer from aggregation and fragmentation effects, which often leads to overestimation of molecular weights, suggesting archipelago architecture. However, very recent mass spectrometric studies have shown that these effects can be minimized by using suitable ionization methods such as laser desorption single-photon ionization (LDSPI)[58] and laser desorption laser ionization (two-step laser or L^{2}MS).[59,60] Results from these studies strongly support the island model and the average molecular weight calculated in this work falls in the range reported by these studies. A final average structure of an aromatic cluster is constructed in Figure 7 using the parameters mentioned in Table 4 with a molecular formula of $C_{48}H_{53}NOS_2$ and a molecular weight of 724.07 g/mol. It cannot be said with certainty from this study how many of such structures form the nanoaggregates, but it was determined from the relaxation measurements that 6−7 nanoaggregates constitute a cluster.

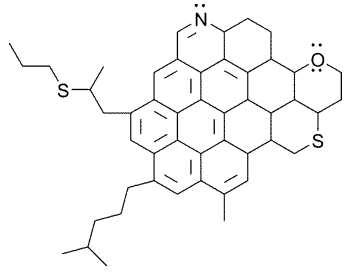

Figure 7. Average structure of an asphaltene molecule constructed using parameters obtained from ^{1}H and ^{13}C NMR spectroscopy. Molecular formula: $C_{48}H_{53}NOS_2$. Molecular weight: 724.07 g/mol.

4. CONCLUSION

The solution-state ^{1}H and ^{13}C NMR spectra of heptane-extracted Athabasca oil-sands asphaltene have been resolved into their respective component peaks by using deconvolution analysis. The peak areas of the various carbon species were obtained from both spectra independently and were found to agree closely. The overlapping peaks in the spectra were revealed with help of the HSQC NMR experiment. The validity of the peak-fitting model was further verified by comparing the H/C ratio obtained from the NMR spectra to that obtained from elemental analysis. Various structural parameters such as size of aromatic clusters, number of substitutions per cluster and average aliphatic chain length were determined. It was found that each polyaromatic cluster is composed of 6−7 aromatic rings, which agrees with the number of rings predicted by the Yen−Mullins model.[17,41] The ^{1}H T_1 and T_2 relaxation parameters of all the moieties were determined, and using the T_1/T_2 ratios it was shown that the asphaltene nanoaggregates and clusters exhibit highly restricted reorientational motion which is two to 3 orders of magnitude slower compared to simpler molecules. The biexponential relaxation behavior of most of the signals revealed that the same moieties can lie in different domains of mobility, which was explained in terms of the Yen−Mullins model, and the percentages lying in the separate domains were also calculated. It was shown that the

dx.doi.org/10.1021/ef401412w | Energy Fuels 2013, 27, 6528−6537

nanoaggregate clusters are small in size, consisting of 6 to 7 nanoaggregates per cluster on average. By modification of the HSQC experimental parameters, it was shown that the alicyclic rings are closely associated with the aromatic core and strong long-range heteronuclear couplings are in exist between them. This study adds to the evidence for the island model as the predominant asphaltene architecture and confirms several structural features proposed by the Yen–Mullins model, using NMR spectroscopy exclusively. However, to get an even better understanding of the dynamics of the asphaltene molecules, nanoaggregates, and clusters, relaxation measurements at different temperatures and different asphaltene concentrations are required, along with further use of 2D correlation NMR spectroscopic methods, which shall be dealt with in future studies.

■ ASSOCIATED CONTENT

Supporting Information

Spectrum showing the effect of turning off the 1-ms trim-pulse in the l-HSQC experiment. This material is available free of charge via the Internet at http://pubs.acs.org.

■ AUTHOR INFORMATION

Corresponding Author

*E-mail: paul.hazendonk@uleth.ca.

Notes

The authors declare no competing financial interest.

■ ACKNOWLEDGMENTS

M.G. and P.H. thank the Natural Sciences and Engineering Research Council of Canada (NSERC) for financial support. We thank Tony Montina, University of Lethbridge NMR manager for his help with setting up the inverse gated decoupling and relaxation sequences and Kevin Johnson for performing the elemental analysis.

■ REFERENCES

(1) Cyr, N.; McIntyre, D. D.; Toth, G.; Strausz, O. P. *Fuel* **1987**, *66*, 1709–1714.
(2) Östlund, J.-A.; Andersson, S.-I.; Nydén, M. *Fuel* **2001**, *80*, 1529–1533.
(3) Ancheyta, J.; Centeno, G.; Trejo, F.; Marroquín, G.; García, J. A.; Tenorio, E.; Torres, A. *Energy Fuels* **2002**, *16*, 1121–1127.
(4) Storm, D. A.; Edwards, J. C.; DeCanio, S. J.; Sheu, E. Y. *Energy Fuels* **1994**, *8*, 561–566.
(5) Bunger, J. W.; Li, N. C., Eds. *Chemistry of Asphaltenes*; Advances in Chemistry Series 195; American Chemical Society: Washington, DC, 1981; pp 1–15.
(6) Calemma, V.; Iwanski, P.; Nali, M.; Scotti, R.; Montanari, L. *Energy Fuels* **1995**, *9*, 225–230.
(7) Murgich, J.; Rodríguez; Aray, Y. *Energy Fuels* **1996**, *10*, 68–76.
(8) Douda, J.; Llanos, M. E.; Alvarez, R.; Franco, C. L.; de la Fuente, J. A. M. *J. Anal. Appl. Pyrolysis* **2004**, *71*, 601–612.
(9) Ortega-Rodriguez, A.; Duda, Y.; Guevara-Rodriguez, F.; Lira-Galeana, C. *Energy Fuels* **2004**, *18*, 674–681.
(10) Strausz, O. P.; Mojelsky, T. W.; Lown, E. M. *Fuel* **1992**, *71*, 1355–1363.
(11) Mojelsky, T. W.; Ignasiak, T. M.; Frakman, Z.; McIntyre, D. D.; Lown, E. M.; Montgomery, D. S.; Strausz, O. P. *Energy Fuels* **1992**, *6*, 83–96.
(12) Artok, L.; Su, Y.; Hirose, Y.; Hosokawa, M.; Murata, S.; Nomura, M. *Energy Fuels* **1999**, *13*, 287–296.
(13) Groenzin, H.; Mullins, O. C. *Energy Fuels* **2000**, *14*, 677–684.
(14) Sabbah, H.; Morrow, A. L.; Pomerantz, A. E.; Zare, R. N. *Energy Fuels* **2011**, *25*, 1597–1604.
(15) Murgich, J.; Abanero, J. A.; Strausz, O. P. *Energy Fuels* **1999**, *13*, 278–286.
(16) Karimi, A.; Qian, K.; Olmstead, W. N.; Freund, H.; Yung, C.; Gray, M. R. *Energy Fuels* **2011**, *25*, 3581–3589.
(17) Mullins, O. C. *Energy Fuels* **2010**, *24*, 2179–2207.
(18) Sheremata, J. M.; Gray, M. R.; Dettman, H. D.; McCaffrey, W. C. *Energy Fuels* **2004**, *18*, 1377–1384.
(19) Dereppe, J. M.; Moreaux, C.; Castex, H. *Fuel* **1978**, *57*, 435–441.
(20) Semple, K. M.; Cyr, N.; Fedorak, P. M.; Westlake, D. W. S. *Can. J. Chem.* **1990**, *68*, 1092–1099.
(21) Christopher, J.; Sarpal, A. S.; Kapur, G. S.; Krishna, A.; Tyagi, B. R.; Jain, M. C.; Jain, S. K.; Bhatnagar, A. K. *Fuel* **1996**, *75*, 999–1008.
(22) Desando, M. A.; Lahajnar, G.; Ripmeester, J. A.; Ivan, Z. *Fuel* **1999**, *78*, 31–45.
(23) Desando, M. A.; Ripmeester, J. A. *Fuel* **2002**, *81*, 1305–1319.
(24) Buenrostro-Gonzalez, E.; Groenzin, H.; Lira-Galeana, C.; Mullins, O. C. *Energy Fuels* **2001**, *15*, 972–978.
(25) Andrews, A. B.; Edwards, J. C.; Pomerantz, A. E.; Mullins, O. C.; Nordlund, D.; Norinaga, K. *Energy Fuels* **2011**, *25*, 3068–3076.
(26) Doddrell, D. M.; Pegg, D. T.; Bendall, M. R. *J. Magn. Reson.* **1982**, *48*, 323–327.
(27) Durand, E.; Clemancey, M.; Quoineaud, A.-A.; Verstraete, J.; Espinat, D.; Lancelin, J.-M. *Energy Fuels* **2008**, *22*, 2604–2610.
(28) Durand, E.; Clemancey, M.; Lancelin, J.-M.; Verstraete, J.; Espinat, D.; Quoineaud, A.-A. *J. Phys. Chem. C* **2009**, *113*, 16266–16276.
(29) Durand, E.; Clemancey, M.; Lancelin, J.-M.; Verstraete, J.; Espinat, D.; Quoineaud, A.-A. *Energy Fuels* **2010**, *24*, 1051–1062.
(30) Sarpal, A. S.; Kapur, G. S.; Chopra, A.; Jain, S. K.; Srivastava, S. P.; Bhatnagar, A. K. *Fuel* **1996**, *75*, 483–490.
(31) Alshareef, A. H.; Scherer, A.; Tan, X.; Azyat, K.; Stryker, J. M.; Tykwinski, R. R.; Gray, M. R. *Energy Fuels* **2011**, *25*, 2130–2136.
(32) Abu-Dagga, F.; Rüegger, H. *Fuel* **1988**, *67*, 1255–1262.
(33) Dosseh, G.; Rousseau, B.; Fuchs, A. H. *Fuel* **1991**, *70*, 641–646.
(34) Jestin, J.; Barré, L. *J. Dispersion Sci. Technol.* **2004**, *25*, 341–347.
(35) Evdokimov, I. N.; Eliseev, N. Y.; Akhmetov, B. R. *Fuel* **2003**, *82*, 817–823.
(36) Evdokimov, I. N.; Eliseev, N. Y.; Akhmetov, B. R. *Fuel* **2006**, *85*, 1465–1472.
(37) Pekerar, S.; Lehmann, T.; Méndez, B.; Acevedo, S. *Energy Fuels* **1998**, *13*, 305–308.
(38) Östlund, J. A.; Löfroth, J. E.; Holmberg, K.; Nyden, M. *J. Colloid Interface Sci.* **2002**, *253*, 150–158.
(39) Mandal, P. K.; Majumdar, A. *Concepts Magn. Reson., Part A* **2004**, *20A*, 1–23.
(40) Meiboom, S.; Gill, D. *Rev. Sci. Instrum.* **1958**, *29*, 688–691.
(41) Mullins, O. C.; Sabbah, H.; Eyssautier, J.; Pomerantz, A. E.; Barré, L.; Andrews, A. B.; Ruiz-Morales, Y.; Mostowfi, F.; McFarlane, R.; Goual, L.; Lepkowicz, R.; Cooper, T.; Orbulescu, J.; Leblanc, R. M.; Edwards, J.; Zare, R. N. *Energy Fuels* **2012**, *26*, 3986–4003.
(42) Kubo, R. *J. Phys. Soc. Jpn.* **1954**, *9*, 935.
(43) Mandal, P. K.; Majumdar, A. *Concepts Magn. Reson., Part A* **2004**, *20*, 1–23.
(44) Kontaxis, G.; Stonehouse, J.; Laue, E. D.; Keeler, J. *J. Magn. Reson., Ser. A* **1994**, *111*, 70–76.
(45) Hansen, P. E. *Prog. Nucl. Magn. Reson. Spectrosc.* **1981**, *14*, 175–295.
(46) Boek, E. S.; Yakovlev, D. S.; Headen, T. F. *Energy Fuels* **2009**, *23*, 1209–1219.
(47) Solum, M. S.; Pugmire, R. J.; Grant, D. M. *Energy Fuels* **1989**, *3*, 187–193.
(48) Zajac, G. W.; Sethi, N. K.; Joseph, J. T. *Scanning Microsc.* **1994**, *8*, 463–470.
(49) Sharma, A.; Groenzin, H.; Tomita, A.; Mullins, O. C. *Energy Fuels* **2002**, *16*, 490–496.
(50) Klee, T.; Masterson, T.; Miller, B.; Barrasso, E.; Bell, J.; Lepkowicz, R.; West, J.; Haley, J. E.; Schmitt, D. L.; Flikkema, J. L.;

Cooper, T. M.; Ruiz-Morales, Y.; Mullins, O. C. *Energy Fuels* **2011**, *25*, 2065−2075.
(51) Pinkston, D. S.; Duan, P.; Gallardo, V. A.; Habicht, S. C.; Tan, X.; Qian, K.; Gray, M.; Müllen, K.; Kenttämaa, H. I. *Energy Fuels* **2009**, *23*, 5564−5570.
(52) Wargadalam, V. J.; Norinaga, K.; Iino, M. *Fuel* **2002**, *81*, 1403−1407.
(53) Badre, S.; Carla Goncalves, C.; Norinaga, K.; Gustavson, G.; Mullins, O. C. *Fuel* **2006**, *85*, 1−11.
(54) Qian, K.; Edwards, K. E.; Siskin, M.; Olmstead, W. N.; Mennito, A. S.; Dechert, G. J.; Hoosain, N. E. *Energy Fuels* **2007**, *21*, 1042−1047.
(55) Groenzin, H.; Mullins, O. C. *J. Phys. Chem. A* **1999**, *103*, 11237−11245.
(56) Andrews, A. B.; Guerra, R. E.; Mullins, O. C.; Sen, P. N. *J. Phys. Chem. A* **2006**, *110*, 8093−8097.
(57) Lisitza, N. V.; Freed, D. E.; Sen, P. N.; Song, Y.-Q. *Energy Fuels* **2009**, *23*, 1189−1193.
(58) Sabbah, H.; Pomerantz, A. E.; Wagner, M.; Müllen, K.; Zare, R. N. *Energy Fuels* **2012**, *26*, 3521−3526.
(59) Wu, Q.; Pomerantz, A.; Mullins, O.; Zare, R. *J. Am. Soc. Mass Spectrom.* **2013**, *24*, 1116−1122.
(60) Pomerantz, A. E.; Hammond, M. R.; Morrow, A. L.; Mullins, O. C.; Zare, R. N. *J. Am. Chem. Soc.* **2008**, *130*, 7216−7217.